FULL PAPER

Combined Chemical Modification and Collision Induced Unfolding Using Native Ion Mobility-Mass Spectrometry Provides Insights into Protein Gas-phase Structure

Asia Al-jabiry,[a] Martin Palmer,[b] James Langridge,[b] Jeddidiah Bellamy-Carter,[a] David Robinson[c] and Neil J. Oldham[a]*

[a] Ms. A. Al-jabiry, Dr J. Bellamy-Carter, Prof. Neil J. Oldham*
School of Chemistry
University of Nottingham
University Park, Nottingham, NG7 2RD, UK
E-mail: neil.oldham@nottingham.ac.uk
Twitter: @NottsChemistry
[b] Dr. M. Palmer, Dr. J. Langridge
Waters Corporation
Stamford Avenue
Altrincham Road, Wilmslow, Cheshire, SK9 4AX, UK
[c] Dr D. Robinson
School of Science and Technology
Nottingham Trent University
Clifton Lane, Nottingham, NG11 8NS, UK

Supporting information for this article is given via a link at the end of the document.

Abstract: Native mass spectrometry is now an important tool in structural biology. Thus, the nature of higher protein structure in the vacuum of the mass spectrometer is an area of significant interest. One of the major goals in the study of gas-phase protein structure is to elucidate the stabilising role of interactions at the level of individual amino acid residues. A strategy combining protein chemical modification together with collision induced unfolding (CIU) was developed and employed to probe the structure of compact protein ions produced by native electrospray ionisation. Tractable chemical modification was used to alter the properties of amino acid residues, and ion mobility-mass spectrometry (IM-MS) utilised to monitor the extent of unfolding as a function of modification. From these data the importance of specific intramolecular interactions for the stability of compact gas-phase protein structure can be inferred. Using this approach, and aided by molecular dynamics simulations, an important stabilising interaction between K6 and H68 in the protein ubiquitin was identified, as was a contact between the N-terminus and E22 in a ubiquitin binding protein UBA2.

Introduction

Native electrospray ionisation-mass spectrometry (ESI-MS) and related techniques are now widely used in structural biology.[1] The preservation of non-covalent protein-protein interactions (PPIs), and protein-small molecule interactions allows protein complexes to be interrogated, and events such as drug binding to be detected and screened. Although these elements of higher-order protein structure survive the electrospray process, which includes both the deposition of net charges and desolvation, there is little doubt that protein structure undergoes some alteration during ionisation and transfer into the solvent-free high-vacuum environment of the mass spectrometer.[2] It is thought that the sidechains of external amino acid residues collapse back onto the surface of the protein as solvent is removed, and that ionic interactions become particularly important in structural stabilisation. That said, in the absence of thermal activation, it may be tens of milliseconds before further, gross structural rearrangement of the protein ensues.[3] This property provides a potential window for observation of 'native-like' biomolecules in a gas-phase environment.

Ion mobility-mass spectrometry (IM-MS), which facilitates separation of gas-phase ions based on shape, mass and charge, is a powerful hyphenated technique for studying protein structure in a solvent-free environment. The mobility, *K*, of ions travelling through a drift cell under the influence of a static electric field, *E*, at the low field limit, is inversely proportional to their collisional cross section (*CCS*).[4] This parameter can be used to deduce information about the folded state of the protein, and compared with theoretical structures derived from gas-phase simulations. Travelling wave ion mobility spectrometry (TWIMS) is a commonly alternative to static-field drift tube ion mobility, and can also be used to determine *CCS* of ions, providing that appropriate calibration is performed.[5] IM-MS has been used to analyse large protein complexes,[6] identify antibody isoforms and their glycoforms,[7] study intrinsically disordered proteins,[8] analyse virus capsid assembly,[9] probe amyloid formation,[10] and study protein-drug interactions.[11]

Ubiquitin (Ub), a small (8.5 kDa) regulatory protein has been studied extensively by IM-MS. Wyttenbach and Bowers have used ion mobility to show that Ub electrosprayed from a neutral

aqueous solution possesses a *CCS* consistent with the native state.[12] Bakhtiari and Konermann used comparison of IM-MS with a mobile-proton molecular dynamics (MD) simulation to demonstrate that the basic native fold is maintained with collapse of the surface sidechain residues, and a weakening of salt bridges relative to the standard Zwitterionic model.[13] The Clemmer group employed an ion trap to store Ub ions in the gas-phase over the 10^{-3} to 10^{1} s timescale prior to mobility analysis, and showed that the 6+ charge state remained compact over the entire time range.[14] Warnke *et al.* have employed IM to conduct conformer selective UV photodissociation (UVPD) on the 7^{+} charge state of Ub.[15] The Barran group have used similar methodology to probe the initial unfolding steps of the 6+ Ub ion under collisional activation,[16] and have also studied the effects of charge state reduction on the conformation of Ub ions.[17] Servage *et al.* have used cryogenic IM-MS to detect a water-mediated Ub-dimer,[18] whilst Ridgeway *et al.* have employed trapped ion mobility to visualise microheterogeneity within conformational states of Ub ions over 6^{+}-13^{+} charge states.[19] The Sobott group have used electron transfer dissociation (ETD) in combination with IM-MS to show that the more extended conformations of Ub are prone to increased dissociation.[20]

Collision induced unfolding (CIU) is a method for studying the unfolding of protein ions in the gas-phase using programmed collisional activation prior to ion mobility analysis.[21] The groups of Jarrold and Clemmer were among the first to apply this approach,[22] although the term CIU was not coined until later, where it was used to demonstrate the stabilisation of protein structure upon ligand binding.[23] The Ruotolo group has applied CIU to many systems, thereby demonstrating its utility in protein structural studies. Examples include protein-ligand structural stabilisation,[24] the effects of anion adduction on structural stability,[25] determination of the number of folded domains in a protein structure,[26] the characterisation of disulfide bonding patterns and glycoforms in antibodies,[27] and distinguishing competitive vs. allosteric kinase inhibitors.[28] Recently, Eldrid *et al.* have utilised a cyclic TWIMS device,[29] developed and commercialised by the Waters Corporation,[30] to study the gas-phase stability and CIU of protein ions. With its high resolving power, and ability to perform IMS^{n} measurement, this platform provided a detailed understanding of unfolding processes of a number of protein systems.

A major goal in the study of gas-phase protein structure is to elucidate the stabilising role of intramolecular interactions at the level of individual amino acid residues. One method of achieving this is to examine mutant proteins and compare their CIU behaviour with the wild type (WT) version. Although such studies have been performed with a small number of isolated mutants, usually designed to address existing structural questions,[31] the systematic use of site directed mutagenesis for CIU stability scanning requires large numbers of variants to be generated for a single protein, which is both time consuming and expensive.

Chemical modification offers a way of altering the chemical properties of amino acid sidechains within proteins. Providing that the site(s) of modification can be tracked and linked to CIU behaviour, this approach would offer a convenient alternative to the preparation of large numbers of mutants. Modifications that are specific to particular amino acids, such as Lys, His, Tyr, Cys and the acidic residues Asp and Glu are known,[32] and offer a means of probing the stabilising roles of these residues within a given gas-phase protein structure.

Here we describe an approach for studying protein structure in the gas-phase that combines chemical protein modification with CIU-IM-MS to (i) alter the chemical properties of selected amino acid sidechains and (ii) interrogate the effects of this change on the stability of the protein's compact structure. From this process, information on the nature of gas-phase protein structure can be deduced.

Results and Discussion

Acetylation of ubiquitin

Nucleophilic amino acid residues, such as lysine K and cysteine C, are susceptible to acetylation in the presence of a suitable acyl donor. Treatment of ubiquitin (Ub, 10 μM) with acetic anhydride (1.5 mM) in aqueous ammonium bicarbonate (50 mM, pH 7.8) under the conditions described in the Experimental section resulted in acetylation of the protein as determined by ESI-MS (see Figure S1). Signals corresponding to one and two acetylations were clearly visible, with no significant difference in charge state distribution between modified and unmodified protein. Since Ub does not possess any C residues, the expected sites of modification were the seven K residues and N-terminal amino group of Ub. To establish the approximate distribution of acetylation over these positions, electron capture dissociation (ECD) of intact monoacetylated Ub was performed on the 11+ charge state of a denatured sample (see Experimental, and Figure S2). Mapping of acetylation sites was classified as approximate because comparison of the ratios of acetylated versus non-acetylated ions for the c and z ion series revealed some quantitative differences between the degree of modification reported by complementary pairs of ions. These were most likely caused by differences in the fragmentation efficiencies of modified and unmodified ions at particular sites, or possibly by some loss of the acetyl group during fragmentation. Acetylation was observed on the N-terminus and all K residues with the exception of K11 (see Figure S1c).

Collision induced unfolding of acetylated Ub

To investigate the effect of acetylation upon the stability of the compact structure of Ub in the gas-phase, CIU was performed on the 5+ charge state (the most abundant charge state under the native MS conditions employed). The partial acetylation observed in Figure S1 made it possible to conduct CIU on acetylated and unacetylated ions from the same sample, thus separating the effects of sample treatment from the presence or absence of protein modification and ensuring identical instrumental conditions during the CIU process. The Ub 5+ ions (unmodified, *m/z* 1714, acetylated *m/z* 1722) were alternately isolated using the quadrupole mass analyser (MS1) of the Synapt HDMS instrument and activated in the trap collision cell (a stacked-ring ion guide containing argon collision gas, and located between the quadrupole and the ion mobility cell) by increasing the applied collision energy.

At low energy (E_{lab} = 30 eV (6 V collision voltage applied to 5+ ion)), the ion mobility drift traces were essentially identical for the modified and unmodified 5+ ions (see Figure 1a). Calibration of the mobility cell using the method described by Ruotolo *et al.* allowed determination of collisional cross section (CCS).[5] Both ions gave a *CCS* of 975 $Å^2$ at peak maximum (quoted as $^{TW}CCS_{N2\rightarrow He}$).[33] The drift traces remained similar for E_{lab} energies

up to 50 eV, but at 60 eV both acetylated (AcWT) and non-acetylated (WT) 5+ ions began to unfold significantly, with the AcWT ion unfolding more than the unacetylated equivalent (see Figure 1b). This difference was characterised by an unresolved shoulder (*CCS* peak maximum at 1110 Å^2) in the AcWT-Ub drift trace that was absent from the unmodified WT-Ub. Repeated measurements showed this difference to be reproducible. The pattern of additional unfolding of the acetylated 5+ ion persisted at E_{lab} = 80 eV (Figure 1c). Drift traces for additional energies are shown in Figure S3.

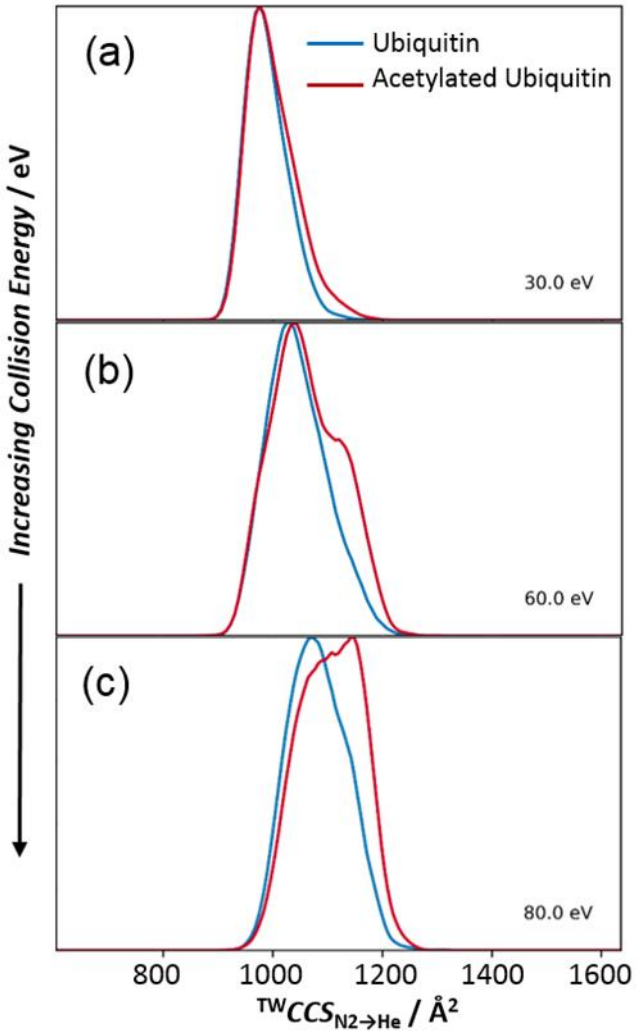

Figure 1. ESI-IM-MS drift traces of the singly acetylated (red) and unacetylated (blue) Ub 5+ ion at collision energies 30, 60 and 80 eV showing destabilisation of the acetylated form.

A comparison of the extent of unfolding of WT-Ub, AcWT-Ub, and a range of other variants described below is shown in Figure 2. The CIU heatmap plots of CCS as a function of collision voltage for Ub and acetylated-Ub are shown in Figure 2a and 2b, respectively. Using the CIUSuite 2.0 package (see Experimental Section), E_{lab} values required for 50 % unfolding, termed CIU_{50}, were extracted and ΔCIU_{50}, the difference between CIU_{50}s for modified and unmodified Ub, calculated. This provided a quantitative measure of (de)stabilisation relative to unmodified WT-Ub, and showed a value of -2.2 (±1.0) eV upon acetylation, which corresponded to significant destabilisation and supported the qualitative data shown in Figure 1. This was further illustrated by a difference plot of the CIU data in Figure 2a and 2b, which is shown in Figure 2d. Here there is a clear tendency for acetylated Ub (blue) to be distributed at higher *CCS* values relative to Ub (red) during the unfolding process (RMSD 12.8 %).

Destabilisation of the compact structure of the Ub 5+ ion as a result of acetylation may be due to modification at different sites on the protein. In order to identify which positions were important in causing destabilisation, a time aligned parallel (TAP) fragmentation experiment was performed. The 5+ AcWT-Ub ion (*m/z* 1722) was quadrupole isolated, partially activated in the trap (70 eV), mobility separated, and fragmented in the transfer region of the Synapt HDMS at high energy (E_{lab} = 450 eV). A series of singly-charged b ions were observed in the resulting mass spectrum (Figure S4a) giving good coverage of the seven N-terminal residues of Ub, and thus allowing investigation of the effects of acetylation at the N-terminus and K6. Plotting the extracted ion drift traces for the modified and unmodified b_5 ions showed similar degrees of unfolding (see Figure S4b), which demonstrated that acetylation at the N-terminus has little effect on the stability of the compact structure. By contrast, similar plots for the b_6 ion showed significantly more unfolding of the modified ion population (see Figure S4c). These results taken together revealed that acetylation at K6 caused significant destabilisation of Ub's gas-phase structure. The absence of other abundant and diagnostic ions in the CID spectrum of Ub made it impossible to study the effects of acetylation at other lysine residues in a similar manner. Nonetheless, the observed behaviour at K6 was both pronounced and interesting, and thus worthy of more detailed study.

To confirm the significance of the effect of sidechain modification at K6, a K6A Ub mutant was utilised. CIU of the 5+ ion of K6A Ub demonstrated noticeable destabilisation relative to the WT protein. As with AcWT-Ub, a shoulder at higher *CCS* was visible in the drift trace, indicating increased unfolding relative to unmodified WT-Ub, but with the K6A mutant this difference appeared at somewhat lower energies (E_{lab} = 10-30 eV, see Figure S5). Figure 2c illustrates the increased extent of unfolding of K6A Ub as a CIU plot, which gave rise to a ΔCIU_{50} value of -14.0 (± 0.5) eV relative to WT-Ub, and is further shown in the difference plot of CIU data in Figure 2e. K6A Ub (blue) displayed a tendency to exhibit larger CCS values that WT-Ub (red) during the unfolding process (RMSD 26.7 %). The increased destabilising effect seen with K6A when compared to acetylated-Ub may result from chemical differences in their sidechains at position 6, or may be due to the homogeneous nature of the mutant at position 6 versus the statistical distribution of acetylation over the K residues and the N-terminus of Ub. In the latter case this means that only 30 % of acetylated-Ub is modified at position 6 (see Figure S1), which dilutes the destabilising effect. The significance of K6 was further supported by use of a K6-only mutant, in which all K residues other than K6 were mutated to R. Comparison of the acetylated and unacetylated versions of this Ub variant showed similar behaviour to WT-Ub, with significant destabilisation accompanying modification (see Figures 2f and g, and S6). The ΔCIU_{50} value between acetylated K6-only and unmodified K6-only was -2.8 (±1.3) eV.

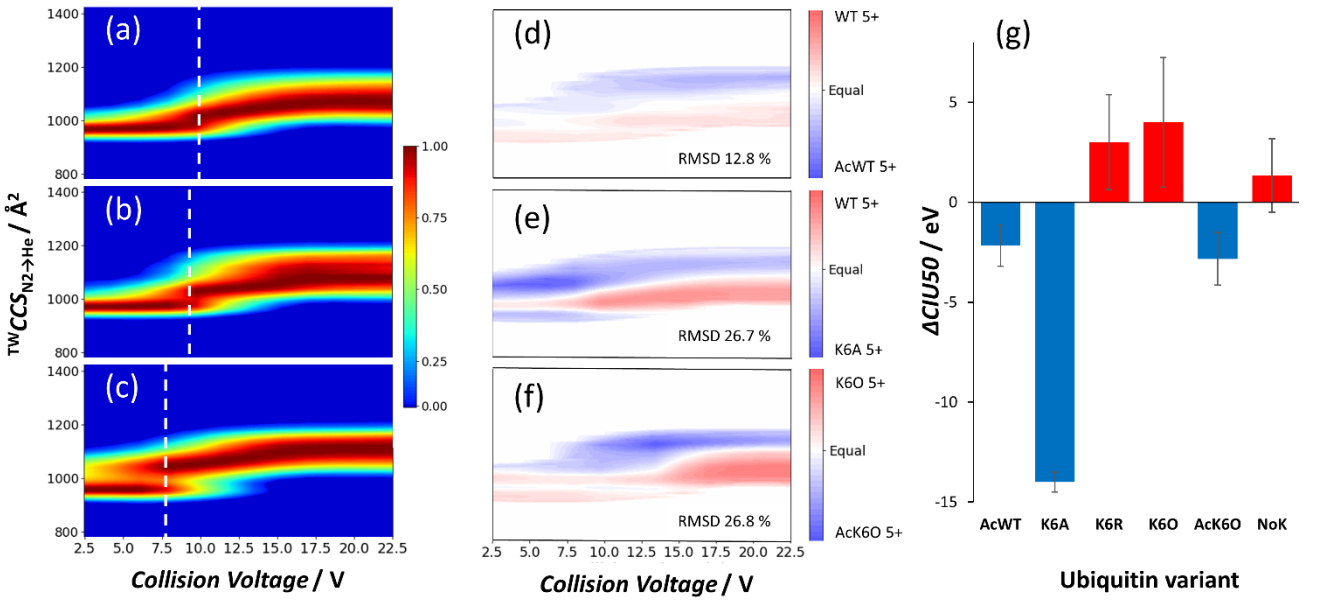

Figure 2. CIU data showing the unfolding of 5+ Ub ions (a) unacetylated WT, (b) acetylated WT, and (c) K6A mutant Ub. Difference plots for unacetylated vs acetylated WT Ub, unacetylated WT vs K6A mutant Ub, and unacetylated vs acetylated K6-only (K6O) Ub are shown in (d), (e) and (f) respectively. ΔCIU_{50} values in (g) reveal increased unfolding due to destabilisation of acetylated WT Ub, K6A Ub and acetylated K6 only Ub. Values are relative to unacetylated WT Ub except for acetylated K6-only Ub, which is relative to unacetylated K6-only Ub (CIU_{50} and hench ΔCIU_{50} values are determined from the product of collision voltage and charge state (here 5)).

Additional evidence for the important role of K6 was provided by acetylation of a K6R Ub mutant. In this form of the protein all K residues except K6 are present. Interestingly, in this case, modification led to no discernible destabilisation of the compact protein structure relative to unmodified K6R Ub (ΔCIU_{50} = 0 eV and see Figure S7). From this finding, it could be deduced that acetylation at K residues other than K6 did not induce structural destabilisation. An important wider conclusion of this result is that the destabilisation seen from acetylation of WT-Ub is not simply due to removal of one of the protein's charge(able) sites, but a phenomenon associated specifically with K6. In addition to the major unfolding transition described above, the 5+ ion of some variants of Ub exhibited a minor unfolding step at ca. *CIU50* = 77 eV, however this was difficult to resolve with the limited resolution available, leading to insignificance in ΔCIU_{50} values.

Although the 5+ ion was the most abundant charge state seen for Ub under the electrospray conditions employed, a 6+ ion with intensity 75% of the 5+ was observed in the spectrum (Figure S1). CIU experiments were performed on this charge state for all the variants described above (see drift traces provided in Figures S8-S11). The 6+ ions did display somewhat better resolved unfolding than the 5+, but the relationships between the modified and unmodified variants were similar, with acetylation-related destabilisation of compact structures readily apparent. The 3-state unfolding of 6+ Ub closely resembled that previously seen for the WT protein by Chen and Russell.[34]

It should be noted that thorough desalting of the sample was found to be important, as sodium adducts led to stabilisation of compact protein structure. The mass shift associated with two Na^+ ions is close to that for acetylation, which may lead to masking of effects due to chemical modification. This consideration was particularly relevant for the 6+ Ub, which showed more adduction.

Tandem IM/IM-MS CIU of Ub

To investigate the CIU process of Ub in further detail we employed tandem IM/IM-MS CIU using the Waters Cyclic IMS instrument.[30] The cyclic IM cell allows mobility-resolved ion packets to be isolated, sent upstream, stored in the pre-array, and reinjected into the ion mobility device for a second round of separation. During the reinjection step ions can be collisionally activated to induce unfolding. With this approach the unfolding profiles of specific CIU conformational peaks can be studied.

Figure 3 shows the IM/IM-MS CIU results for the Ub 6+ ion. This charge state was more abundant using the Cyclic IMS instrument and showed more resolved peaks than the 5+ and was chosen for these reasons. Figure 3a is composed of the superimposed CIU IM drift traces of Ub 6+ at E_{lab} 12, 60 and 132 eV to illustrate the principal distributions seen. Figs 3b-3d show the IM/IM-MS CIU heat maps for three isolated ion packets, taken as time slices from primary CIU IM separations, and activated with increasing energy during reinjection. In Figure 3b the compact conformation was isolated and activated to yield essentially the same unfolded species seen in the primary CIU trace (Figure 3a). Isolation and activation of partially unfolded conformations, as shown in Figures 3c and 3d, produced the more unfolded species seen in the primary CIU trace and in Figure 3b. These results show that the unfolding of Ub ions under CIU is a sequential stepwise process with compact conformations producing partially unfolded intermediates which then, with an increase in collision energy, lead to more unfolded forms. Interestingly, no sign of refolding of the partially unfolded species to more compact structures was

observed as evidenced by the absence of ions of lower drift times than those isolated in Figures 3c and 3d, even at low reactivation energies. This indicated that although unfolding may be a theoretically reversible process, under the conditions employed, the activation barrier to refolding to compact structures may be too high on the timeframe used, or that ions retained too much internal energy to refold. Thermal solution-phase unfolding of Ub, measured by IM-MS, was found to be reversible.[35]

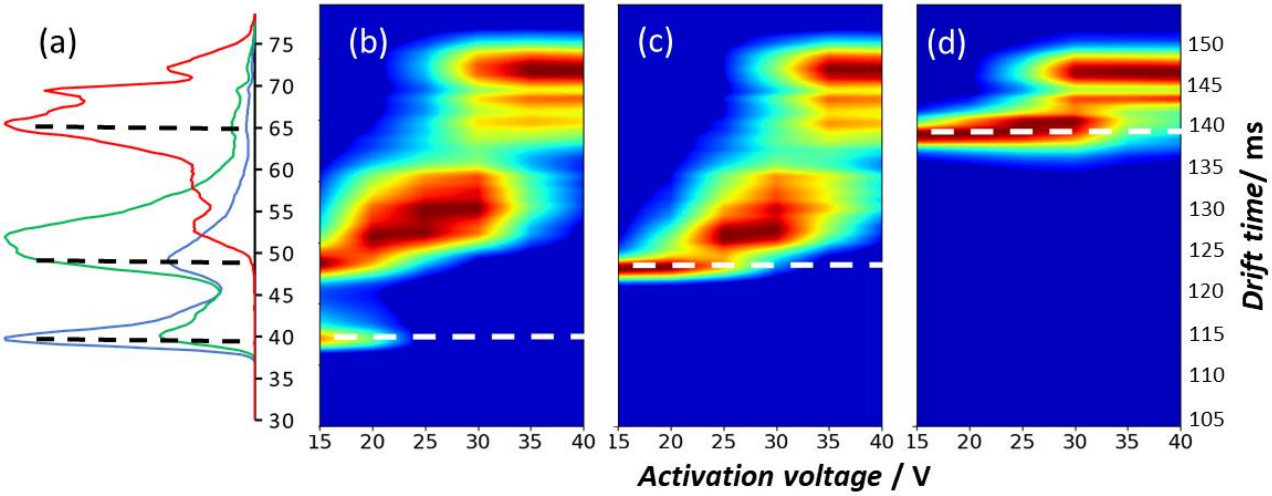

Figure 3. IM/IM-MS CIU of WT Ub 6+ showing (a) primary CIU of the 6+ Ub ion at 12 (blue), 60 (green) and 132 (red) eV trap activation, and IM/IM CIU following isolation and secondary activation of (b) compact conformation (39 ms), (c) intermediate conformation (49 ms) and (d) extended conformation (65 ms). Dotted lines indicate the time slices for selection of precursor ion packets in (a), and are translated to (b), (c) and (d), respectively.

Molecular dynamics simulations

The results obtained so far indicated that, for the 5+ and 6+ ions of Ub, the presence of an unmodified basic lysine residue at position 6 was important in stabilising the compact gas-phase structure. In order to interpret this result, gas-phase molecular dynamics (MD) simulations were performed on the 5+ and 6+ Ub ions. Even a small protein, such as Ub, contains many potential charge sites, and identifying where net charges reside can be challenging. Recently, the Konermann group has elucidated the charge site distribution of native gas-phase Ub ions.[13] Using a mobile proton MD model of 6+ Ub ions, the probabilistic distribution of charges was identified. These results were used to inform MD simulations conducted here. PDB structure 1UBQ was selected as the initial coordinate file. In this structure, and under physiological conditions, Ub was overall neutral in charge. All K and R sidechains, and the N-terminus, were protonated, whilst all D and E sidechains and the C-terminus were deprotonated. The 6+ ion was produced from this structure by reprotonating the sidechains of residues E18, E24, D32, D39, E51, D58 and E64, and deprotonating K63, following the results of Konermann *et al*. (Figure S12a). The 5+ ion was then generated by leaving E18 deprotonated (Figure S12b), as – of the overall neutral acidic residues in the 6+ structure – this position showed the highest probability of carrying a charge by being deprotonated. Recently we have developed a Python-based charge placement algorithm entitled 'ChargePlacer' which provides a general tool for predicting charge sites on protein ions.[36] Using the charge sites listed above, MD simulations were run either at 298 K to produce low energy gas-phase structures, or 750 K in order to induce unfolding. MD was run in two stages: an equilibration run was performed for approximately 0.5 ns, and a production run for approximately 8 ns. All simulations were performed in triplicate. Collisional cross sections were calculated for resulting structures using the corrected PA method, where the *CCS* determined by projection approximation (PA) is converted into the apparent trajectory model (TM) value using a constant scaling $^{factor[1,37]}$ as described in the Experimental section, and mean values for the 3 repeats are presented.

Figure 4 (a-c) shows the experimental drift traces for 5+ WT-Ub CIU at 30, 70 and 110 eV with the plots from the MD simulations shown below. The simulation at 298 K (Figure 4d) was found to be in close agreement with the experimental drift trace at 30 eV, although the former exhibited a narrower distribution of *CCS* values. The peak maximum of the simulated drift trace, at 950 Å^2 was similar to the experimentally determined value of 975 Å^2. A representative MD output structure for a 950 Å^2 *CCS* is shown in as an insert. With the exception of some collapse of the polar sidechain residues back onto the structure, and folding in of the C-terminus, the gas-phase structure retained the basic secondary and tertiary structure of the condensed phase protein. These values are consistent with those previously reported for low charge states of Ub.[12] The 70 eV CIU drift trace exhibited both a shift in *CCS* (peak maximum 1038 Å^2) and a broadening of the peak (Figure 4b). The structure taken from the equilibration phase of the MD simulation at 750 K proved to be a reasonable approximation to this collision energy step (peak maximum 1039 Å^2), albeit with a narrower distribution (Figure 4e). A representative MD output structure for a 1039 Å^2 *CCS* is shown

as an insert. Much of the native secondary structure had broken down. The core hydrophobic residues began to migrate outwards, and the polar hydrophilic residues moved inwards. At 110 eV the drift trace distribution moved still further to higher *CCS*, with a peak maximum of 1083 Å^2 (Figure 4c).

The production run of the MD simulation at 750 K was similar to this high collision energy (peak maximum 1099 Å^2, Figure 4f, representative structure from the MD simulation is shown). The native secondary structure was now lost, and the protein inverted, with many of the polar amino acid sidechains on the interior of the structure and the core hydrophobic residues exposed on the surface. The MD simulations appear qualitatively similar to those seen by Chen and Russell for 6+ Ub ions.[34]

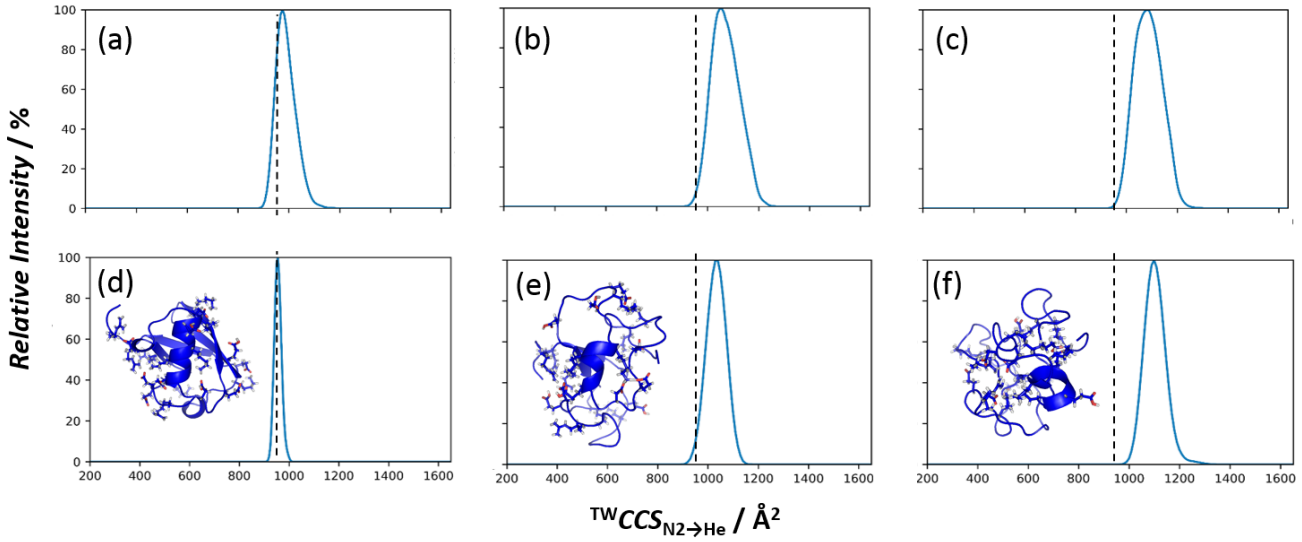

Figure 4. Experimental CIU drift traces for WT Ub 5+ ion at (a) 30 eV, (b) 70 eV and (c) 110 eV, and MD simulations of the WT Ub 5+ charge state at (d) 298 K (0.5 ns), (e) 750 K (0.5 ns) and (f) 750 K (9 ns). Inserts in (d)-(f) show representative MD structures corresponding to the most abundant *CCS* values with chargeable residues K, R, D and E shown as sticks. Dotted lines show *CCS* of the compact theoretical structure (950 Å^2) in all plots as a reference marker.

MD simulations were performed on the K6A Ub 5+ ion using a similar approach to the WT. The absence of a cationic residue in position 6 of this mutant made it necessary to add an additional charge by neutralising E18, as for the 6+ WT-Ub ion. This strategy was both a reasonable approximation to the charge state locations determined by Konermann and coworkers,[13] and also allowed direct comparison between analogous 5+ and 6+ WT ions and 5+ K6A. A plot of the RMSD from the initial coordinates of the atoms in the starting structures for these three species against time for the equilibration run of the 750 K MD simulations revealed interesting differences (Figure S13). The K6A Ub mutant 5+ ion showed significantly more deviation from the initial structure than the WT 5+ ion and, interestingly, also than the WT 6+ ion. Thus, the absence of a (charged) K residue at position 6 appeared to destabilise the structure. This was further supported by simulations on 5+ WT Ub with a neutral K6 (once again with a neutral E18 to give an overall 5+ charge). This structure unfolded more than the 5+ WT bearing a charge on K6, and to a similar extent to K6A Ub.

Examination of the output structures from the equilibration stage of the simulation revealed apparent differences in the distance between residue 6 (K or A) and H68 for the four variants described above. This stage of the MD simulation was chosen as it shows the first steps in unfolding of the compact structures, and hence breaking of the key interactions. To provide a more quantitative interpretation, the inter-residue distance was measured and plotted over for the equilibration run of the MD simulation for each form of Ub (Figure 5a). As with the overall RMSD values, plotting the residue K6-H68 distances led to the four Ub simulations producing two types of behaviour. The 5+ and 6+ WT structures with charged K6 maintained an inter-residue distance of 5-8 Å (mean values 4.9 ± 0.9 Å and for 5+, and 7.9 ± 2.4 Å and for 6+, between 0.25 and 0.5 ns of the simulation). The 5+ K6A mutant, and 5+ WT ion with a neutral K6, in contrast, showed much larger distances over the period 0.25-0. 5 ns (19.2 ± 3.1 Å for 5+ K6A, and 19.9 ± 2.5 Å and for 5+ WT with neutral K6). Example structures are shown in Figure 5b.

Taken together, these results point to the importance of an interaction between protonated K6 and H68 in stabilisation of the compact fold of Ub in the gas-phase. Modification or direct neutralisation of K6 appeared to weaken this interaction and allowed unfolding of the N-terminal β–hairpin of Ub (Figure 5b).

Histidine modification by diethyl pyrocarbonate (DEPC). MD simulations of the 5+ charge state of Ub predicted a role for H68 in stabilising the compact structure of Ub ions in the gas-phase. Histidine modification of the protein was performed to assess its potential impact on stability. Diethyl pyrocarbonate (DEPC) is known to react with histidine residues selectively,[32a] although some reactivity at lysine, cysteine and tyrosine is also reported. DEPC is an electrophile that is able to acylate the imine nitrogen atom of histidine's imidazole ring with an ethoxycarbonyl group. Subsequent deprotonation of the pyrrole-like nitrogen neutralises the iminium and regenerates the tautomeric imidazole ring, with the ethoxycarbonyl group on the newly generated pyrrole-like nitrogen (Figure S14).

Treatment of Ub with DEPC, as described in the Experimental section led to multiple ethoxycarbonyl modifications. Isolation and ECD MS/MS fragmentation of singly-modified Ub identified H68 as the site of carbamoylation (Figure S15), in line with predicted specificity (Ub possesses only a single H residue). Interestingly, when subjected to CIU, the 5+ ion of H68-modified Ub showed some destabilisation relative to its unmodified equivalent (Fig. S16). The ΔCIU_{50} value of -2.0 eV was modest, but significant as unfolding was performed simultaneously on modified and unmodified Ub ions from the same sample. Single DEPC-modification of histidine does not, however, prevent the imine nitrogen from acting as an H-bond acceptor and so there may well still be some K6-H68 interaction in the ion.

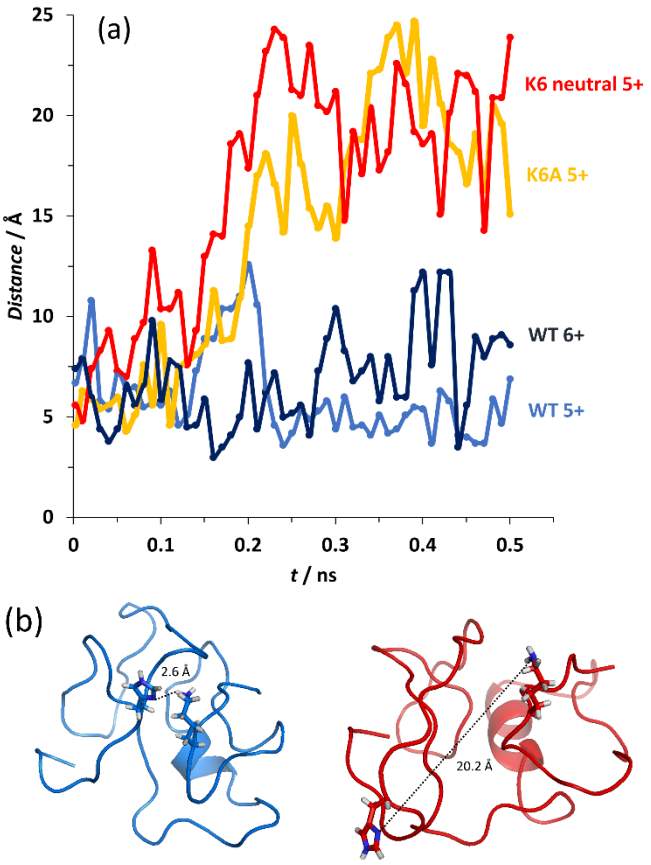

Figure 5. (a) Plot of K6-H68 distance over the 0.5 ns equilibration stage of MD simulations for WT 5+ and WT 6+ Ub, WT 5+ Ub with neutral K6, and K6A 5+ Ub showing increased unfolding with a neutral residue in position 6. Data represent the mean of 3 repeat simulations. (b) Structures of WT Ub 5+ with charged (blue) and neutral (red) K6 (taken at 0.4 ns) showing increased unfolding of the N-terminal β–hairpin in the latter.

Examination of the ECD MS/MS spectrum of doubly ethoxycarbonyl-modified Ub indicated that the lysine residues were the next sites of attachment. CIU of the 5+ ion of this species showed further destabilisation of the compact structure: likely due to some modification at K6 (Figure S17). Signals for the 6+ modified ions were too weak to generate reproducible CIU plots.

Succinylation of Ub. A third protein modification examined was succinylation. An interesting feature of anhydride ring opening by nucleophilic lysine groups is the conversion of a basic amine functionality to an acidic one (Figure S18). Treatment of Ub with succinic anhydride led to efficient modification. Interestingly, in contrast to acetylation, the first modification was found to go exclusively on the N-terminal amino group (Figure S19). Quadrupole isolation and CIU of the 5+ charge state showed that mono-succinylation produced no discernible destabilisation of the protein structure (Figure S20, $\Delta CIU_{50} < 1$ eV). This suggested that modification of the N-terminus, even by a group that changes the polarity of the position, is not detrimental to the stability of the compact gas-phase structure of Ub. In contrast, a second succinylation of the protein was found to provide minor stabilisation of the structure (Figure S21). Signals for the 6+ modified ions were too weak to generate reproducible CIU plots.

Acetylation of UBA2

Although this paper is primarily concerned with chemical modification and CIU of Ub, to investigate whether similar effects were exhibited with other systems, a second protein was examined. The Ub-associating (UBA) domain from the nucleotide excision repair protein hHR23A is a small three-helix bundle suitable as a model for this work.[34] ESI-MS of the protein from ammonium acetate (20 mM) gave principally the 4+ and 5+ charge states. Following acetylation under the conditions described for Ub, CIU was performed on the modified and unmodified protein ions. Results for the 5+ charge state showed distinct destabilisation of the acetylated protein relative to the unacetylated form (Figure S22). In fact, the former was fully unfolded even at the lowest CIU activation level, and the drift trace was identical to that obtained for the ammonium adduct of the UBA previously measured and discussed in a publication from our laboratory.[37b] In that paper it was postulated that ammonium adduction displaced an ionic interaction important in stabilising the compact fold of the gas-phase protein. This was difficult to evidence with a labile adduct, but with covalent acetylation, the disruption of a stabilising intramolecular interaction was potentially tractable. CID MS/MS of intact acetylated UBA2 located the site of acetylation almost exclusively to the N-terminus (Figure S23). In the condensed-phase structure of UBA, the N-terminus has the potential to form an intramolecular salt bridge with E22. Ammonium adduction at E22 would be expected to have a similar disruptive effect on stability of the compact protein structure by displacing this intramolecular interaction (Figure S24). Thus, by modification of a known residue it has been possible to explain destabilisation based on ammonium adduction.

Conclusion

Chemical modification of proteins followed by CIU shows significant promise as a method for studying the stabilising role of intramolecular interactions within gas-phase protein structures. To achieve amino acid-level resolution it is necessary to link unfolding measured by IM-MS to modification on specific residues. In the case of Ub this was achieved by a TAP experiment implicating K6, and with UBA2 by the high degree of acetylation on the N-terminus. It is noteworthy that although K6 appears important in stabilising compact Ub ions in the gas-phase, this residue points out into bulk water in the solution-phase and does not appear to play a role in structural stabilisation in that environment. Thus, differences between the phases are apparent.

Instrumental developments that allow improved protein fragmentation post-IM separation, such as electron transfer dissociation (ETD), will enable identification of stabilising residues in systems where advantageous CID fragmentation or selective reactivity is not seen. This will widen the scope of the methodology and provide new insights into protein structure in the gas-phase.

Experimental Section

Materials

Wild type ubiquitin (bovine) was purchased from Sigma-Aldrich (Merck, Dorset, UK). Recombinant WT Ub and K6A mutant, expressed in *E. coli*, were provided by R. Layfield, University of Nottingham. K6R, 'no K' (K6/11/27/29/33/48/63R) and 'K6 only' (K11/27/29/33/48/63R) Ub mutants were purchased from Boston Biochem (Boston, USA). hHR23A UBA2 was recombinantly expressed in *E. coli* as previously described.[48] Acetic anhydride was purchased from Sigma-Aldrich (Poole, UK), diethyl pyrocarbonate (DEPC) from VWR (Lutterworth, UK), and succinic anhydride, ammonium acetate and ammonium bicarbonate were sourced from Sigma-Aldrich (Poole, UK). Zeba™ Spin Desalting Columns (7KDa MWCO, 0.5 mL) were purchased from ThermoFisher Scientific (Loughborough, UK). MilliQ ultrapure water (Millipore Integral MilliQ system, Watford, UK) was used for all solutions.

Protein sample preparation

Ub and UBA2 samples were desalted into either ammonium acetate (25 mM) or ammonium bicarbonate (50 mM) using Zeba™ Spin Desalting Columns following the manufacturer's instructions. Thorough desalting was found to be particularly important for acetylated samples as the double sodium adduct ion (+ 44 Da) was very close in mass to the acetylated ion (+ 42 Da), and sodium adduction was found to reduce unfolding of the protein ions. ESI-MS spectra for all variants, including spectra of quadrupole-isolated 5+ and 6+ ions for CIU, are shown in Figure S25.

CIU IM-MS experiments

CIU ESI-IM-MS experiments were performed using a Synapt G1 HDMS (Waters Corporation, Wilmslow UK) equipped with a standard electrospray ionisation (ESI) source operated in the positive ion mode. A capillary voltage of 2.5 kV was employed together with a sample cone voltage of 20 V and an extraction cone voltage of 3 V. The source temperature was 50 ˚C. The backing pressure in the intermediate vacuum region of the source was adjusted to 3.8 mbar to provide collisional cooling and increase ion transmission. Protein solutions (5-10 µM) in either ammonium bicarbonate or ammonium acetate (50 mM) were infused at a flow rate of 5 µL min^{-1}. Precursor ions (5+ and 6+) were quadrupole isolated prior to CIU. A wave height of 7 V and a velocity of 280 ms^{-1} was used for the TWIMS cell, which contained nitrogen gas at a pressure of 0.5 mbar. CIU was induced in the trap region (DC bias 10 V), which contained argon as a collision gas at 2 x 10^{-2} mbar, by increasing the collision energy voltage from 2-30 V. Time aligned parallel (TAP) fragmentation experiments were conducted on 5+ acetylated Ub ion using a trap collision energy of 70 eV (14 V) to induce partial unfolding and a transfer collision energy of 450 eV (90 V) to fragment the ions. Data were processed and displayed using MassLynx 4.1 (Waters, Wilmslow, UK) and CIU Suite 2 using parameters: Savitzky-Golay Smoothing, Window 9, Minimum Feature Length 5 Steps, and Feature Allowed Width 20 $Å^2$. Defaults were used for all other parameters.[35] Transition plots for all variants are shown in Figures S26 and S27. Calibration of the TWIMS cell was performed as described by Bush *et al*,[5] using bradykinin, ubiquitin, cytochrome C and myoglobin (Figure S28). All experimental *CCS* values are quoted as $^{TW}CCS_{N2\rightarrow He}$.[33]

CIU IM/IM-MS experiments

CIU IM/IM-MS was performed using a SELECT SERIES Cyclic IM-MS instrument (Waters Corporation, Wilmslow UK) equipped with a standard electrospray ionisation (ESI) source operated in the positive ion mode. A capillary voltage of 2.5 kV was employed. Ubiquitin solution (5 µM) in ammonium acetate (50 mM) was infused at a flow rate of 5 µL min^{-1}. Ub 5+ (*m/z* 1714) and 6+ (*m/z* 1428) ions were quadrupole isolated prior to activation. Trap collision voltages of 2, 18 and 26 V for the 5+ ion, and 2, 10 and 22 V for the 6+ ion were used to generate partial unfolding for the first round of IMS separation with the cyclic IMS cell (containing nitrogen gas) used in single pass mode. Following separation, selected ion packets were 'time sliced' using a window of 2.5 ms, stored in the pre-array store to facilitate removal of remaining ions from the cyclic cell and reinjected at energies of 15-40 V (5 V intervals) to initiate secondary CIU prior to the second round of IMS separation. Data were processed and displayed using MassLynx 4.1 (Waters, Wilmslow, UK), and using CIU suite 2.[35]

ECD MS/MS experiments

ECD MS/MS used to identify the sites of protein modification (acetylation, ethoxycarbonoylation and succinylation) was performed on a ThermoFisher Scientific (Hemel Hempstead, UK) LTQFT Ultra hybrid ion trap Fourier transform ion cyclotron resonance (FTICR) MS. Following protein modification, as described below, samples were denatured by the addition of 1-volume equivalent of acetonitrile containing 0.2 % formic acid and analysed using static nanoESI with tips made in-house from borosilicate capillary tubes fitted with a Pt wire electrode attached to a 1.5 kV supply. Modified ions were selected in the ion trap, and ECD performed in the ICR cell using a relative electron energy of 1-1.5 and a reaction time of 100-200 ms. Data were displayed and deconvoluted using Xcalibur software (ThermoFisher Scientific, Hemel Hempstead, UK).

Protein chemical modification

Acetylation. To a solution of the desalted protein (Ub or UBA2, 10 µM) in ammonium bicarbonate (50 mM), acetic anhydride was added to give a final concentration of 1.5 mM. The mixture was incubated at room temperature for 15 min prior to direct measurement by ESI-IM-MS.

Ethoxycarbonylation. To a solution of desalted Ub (10 µM) in ammonium bicarbonate (50 mM) at 4 ˚C, a freshly prepared solution of diethylpyrocarbonate (DEPC) in acetonitrile was added to give a final concentration of 100 µM. The mixture was incubated at 4 ˚C for 5 min prior to direct measurement by ESI-IM-MS.

Succinylation. To a solution of desalted Ub (10 µM) in ammonium bicarbonate (50 mM), a freshly prepared solution of succinic anhydride in (in ammonium bicarbonate (50 mM)) was added to give a final concentration of 1 mM. The mixture was incubated at room temperature for 15 min prior to direct measurement by ESI-IM-MS.

Molecular dynamics simulations

Gas-phase MD simulations were performed on WT and K6A Ub using PDB structure 1UBQ as a starting point for the coordinates. The 5+ and 6+ charge states were generated as follows: WT 5+ ion – neutralisation of residues E24, D32, D39, E51, D58 and E64, and K63; WT 6+ ion – neutralisation of residues E18, E24, D32, D39, E51, D58, E64, and K63; K6A 5+ ion – neutralisation of residues E18, E24, D32, D39, E51, D58, E64, and K63, WT neutral K6 5+ ion – neutralisation of residues E18, E24, D32, D39, E51, D58, E64, K6 and K63. Simulations were run at either 298 K or 750 K in two runs: a 0.5 ns equilibration run, in which the temperature was gradually raised to the target temperature, and a ca. 9 ns production run using the CHARMM36 force field.[39] A timestep of 2 fs was employed.

Three independent simulations were performed on each system. Results were visualised using VMD,[40] and converted to PDB file format for viewing in Pymol.[41] All simulations were performed with CHARMM,[42] using the Minerva high performance computing (HPC) facility at the University of Nottingham and the Hamilton HPC facility at Nottingham Trent University. Collisional cross sections (CCSs) were determined for output structures employing the projection approximation (PA) model using CCSCalc software (Waters Corporation, Wilmslow UK). These CCS_{PA} values were multiplied by the empirically determined scaling factor 1.14 to give the reported, apparent trajectory method (TM) CCS values, as the PA method is known to underestimate the CCS of macromolecules by this factor.[1,37]

Acknowledgements

We are grateful to Qatar University for funding AAJ, to BBSRC for a studentship to JB-C (BB/M008770/1), and to the Faculty of Science, University of Nottingham for a PEF award. We thank UoN and NTU for provision of HPC services on which the MD simulations were performed

Keywords: protein chemical modification • collision induced unfolding • ion mobility-mass spectrometry • native mass spectrometry • protein molecular dynamics

[1] J. L. P. Benesch, B. T. Ruotolo, *Curr. Opin. Struct. Biol.* **2011**, *21*, 641-649.

[2] K. Breuker, F. W. McLafferty, *Proc. Natl. Acad. Sci. USA* **2008**, *105*, 18145-18152.

[3] E. R. Badman, C. S. Hoaglund-Hyzer, D. E. Clemmer, *Anal. Chem.* **2001**, *73*, 6000-6007.

[4] H. E. Revercomb, E. A. Mason, *Anal. Chem.* **1975**, *47*, 970-983.

[5] M. F. Bush, Z. Hall, K. Giles, J. Hoyes, C. V. Robinson, B. T Ruotolo, *Anal. Chem.* **2010**, *82*, 9557-9565.

[6] a) B. T. Ruotolo, K. Giles, I. Campuzano, A. M. Sandercock, R. H. Bateman, C. V. Robinson, *Science* **2005**, *310*, 1658-1661; b) B. T. Ruotolo, J. L. Benesch, A. M. Sandercock, S. J. Hyung, C. V. Robinson, *Nat. Protoc.* **2008**, *3*, 1139-1152; c) A. Politis, A. Y. Park, S. J. Hyung, D. Barsky, B. T. Ruotolo, C. V. Robinson, *PLoS ONE* **2010**, *5*, e12080.

[7] K. Hansen, A. M. Lau, K. Giles, J. M. McDonnell, W. B. Struwe, B. J. Sutton, A. Politis, *Angew. Chem. Int. Ed.* **2018**, *57*, 17194-17199.

[8] a) T. W. Knapman, N. M. Valette, S. L. Warriner, A. E. Ashcroft, *Curr. Anal. Chem.* **2013**, *9*, 181-191; b) D. Stuchfield, P. Barran, *Curr. Opin. Chem. Biol.*, 2018, *42*, 177-185.

[9] a) C. Uetrecht, I. M. Barbu, G. K. Shoemaker, E. van Duijn E, A. J. Heck, *Nat. Chem.* **2011**, *3*, 126-132; b) D. A. Shepherd, K. Holmes, D. J. Rowlands, N. J. Stonehouse, A. E. Ashcroft, *Biophys. J.* **2013**, *105*, 1258-1267.

[10] a) C. Bleiholder, N. F. Dupuis, T. Wyttenbach, M. T. Bowers, *Nat. Chem.* **2011**, *3*, 172-177; b) L. M. Young, P. Cao, D. P. Raleigh, A. E. Ashcroft, S. E. Radford, *J. Am. Chem. Soc.* **2014**, *136*, 660-670.

[11] C. E. Eyers, M. Vonderach, S. Ferries, K. Jeacock, P.A. Eyers *Curr. Opin. Chem. Biol*. **2018**, *42*,167-176.

[12] T. Wyttenbach, M. T. Bowers, *J. Phys. Chem. B* **2011**, *115*, 12266-12275.

[13] a) M. Bakhtiari, L. Konermann, *J. Phys. Chem.* B **2019**, *123*, 1784-1796; b) L. Konermann, E. Aliyari, J. H. Lee, *J. Phys. Chem. B* **2021**, *125*, 3803-3814.

[14] S. Myung, E. R. Badman, Y. J. Lee, D. E. Clemmer, *J. Phys. Chem. A* **2002**, *106*, 9976-9982.

[15] S. Warnke, G. von Helden, K. Pagel, Proteomics **2015**, *15*, 2804-2812.

[16] A. Theisen, R. Black, D. Corinti, J. M. Brown, B. Bellina, P. E. Barran, *J. Am. Soc. Mass Spectrom.* **2019**, *30*, 24-33.

[17] J. R. Jhingree, P. E. Barran, *ChemRxiv*, **2017**.

[18] K. A. Servage. J. A. Silveira, K.L. Fort, D. E. Clemmer, D. H. Russell, *J. Phys. Chem. Lett.* **2015**, *62*, 4947-4951.

[19] M. E. Ridgeway, J. A. Silveira, J. E. Meiera, M. A. Park, *Analyst*, **2015**, *140*, 6964-6972.

[20] F. Lermyte, M. Krzysztof Łącki, D. Valkenborg, A. Gambin, F. Sobott, *J. Am. Soc. Mass Spectrom.* **2017**, *28*, 69-76.

[21] S. M. Dixit, D. A. Polasky, B. T. Ruotolo, *Curr. Opin. Chem. Biol.* **2018**, *42*, 93-100.

[22] a) K. B. Shelimov, D. E. Clemmer, R. R. Hudgins, M. F. Jarrold, *J. Am. Chem. Soc.* **1997**, *119*, 2240-2248; b) S. J. Valentine, J. G. Anderson, A. D. Ellington, D. E. Clemmer, *J. Phys. Chem. B* **1997**, *101*, 3891-3900.

[23] J. T. S. Hopper, N. J. Oldham, *J. Am. Soc. Mass Spectrom.* **2009**, *20*, 1851-1858.

[24] a) S.-J. Hyung, C. V. Robinson, B. T. Ruotolo, *Chem. Biol.* **2009**, *16*, 382-390; b) S. Niu, B. T. Ruotolo, *Protein Sci.*, **2015**, *24*, 1272-1281.

[25] L. Han, S.-J. Hyung. J. J. S. Mayers, B. T. Ruotolo, *J. Am. Chem. Soc.* **2011**, *133*, 11358-11367.

[26] Y. Zhong, L. Han, B. T. Ruotolo, *Angew. Chem. Int. Ed.* **2014**, *53*, 9209-9212.

[27] a) Y. Tian, L. Han, A.C. Buckner, B.T. Ruotolo, *Anal. Chem.* **2015**, *87*, 11509-11515; b) Y. Tian, B.T. Ruotolo, *Int. J. Mass Spectrom.* **2018**, *425*, 1-9.

[28] J. N. Rabuck-Gibbons, J. E. Keating, B. T. Ruotolo, *Int. J. Mass Spectrom.* **2018**, *427*, 151-156.

[29] C. Eldrid, J. Ujma, S. Kalfas, N. Tomczyk, K. Giles, M. Morris, K. Thalassinos, *Anal. Chem*. **2019**, *91*, 7554-7561.

[30] K. Giles, J. Ujma, J. Wildgoose, S. Pringle, K. Richardson, D. Langridge, M. Green, *Anal. Chem.* **2019**, *91*, 8564-8573.

[31] a) O. Hernandez-Alba, E. Wagner-Rousset, A, Beck, S. Cianférani, *Anal. Chem.* **2018**, *90*, 8865-8872; b) H. Wang, J. Eschweiler, W. Cui, H. Zhang, C. Frieden, B. T. Ruotolo, M. L. Gross, *J. Am. Soc. Mass Spectrom.* **2019**, *30*, 876-885; c) A. N. Calabrese, S. E Radford, *Methods* **2018**, *147*, 187-205; d) S. A. Marrella, K. A. Brown, F. Mansouri-Noori, J. Porat, D. J. Wilson, M. A. Bayfield, *J. Biol. Chem.* **2019**, *294*, 1529-1540.

[32] a) E. Baslé, N. Joubert, M. Pucheault, *Chem. Biol*. **2010**, 17, 213-227; b) V.L. Mendoza, R. W. Vachet, *Mass Spectrom. Rev.* **2009**, *28*, 785-815; c) C. D. Spicer, B. G. Davis, *Nat. Comm.* **2014**, *5*, 4740.

[33] V. Gabelica, A. A. Shvartsburg, C. Afonso, P. Barran, J. L. P. Benesch *et al. Mass Spectrom. Rev.* **2019**, *38*, 291-320.

[34] S.-H. Chen, D. H. Russell, *J. Am. Soc. Mass Spectrom.* **2015**, *26*, 1433-1443.

[35] T. J. El-Baba, D. W. Woodall, S. A. Raab, D. R. Fuller, A. Laganowsky, D. H. Russell, D. E. Clemmer, *J. Am. Chem. Soc.* **2017**, *139*, 6306–6309.

[36] J. Bellamy-Carter, L. O'Grady, M. Passmore, M. Jenner, N. J. Oldham, *Analysis & Sensing*, **2021**, *1*, 63 –69.

[37] a) K. Sokratous, R. Layfield, N. J. Oldham, *Int. J. Ion Mobil. Spectrom.* **2013**, *16*, 19-27; b) K. Sokratous, L. V. Roach, D. Channing, J. Strachan, J. Long, M. S. Searle, R. Layfield, N. J Oldham, *J. Am. Chem. Soc.* **2012**, *134*, 6416-6424.

[38] D. A. Polasky, S. M. Dixit, S. M. Fantin, B. T. Ruotolo, *Anal Chem.* **2019**, *91*, 3147-3155.

[39] J. Huang, A. D. MacKerell Jr., *J. Comp. Chem.* **2013**, *34*, 2135-2145.

[40] W. Humphrey, A. Dalke, K. Schulten, *J. Molec. Graphics* **1996**, *14*, 33-38.

[41] The PyMOL Molecular Graphics System, Version 2.0 Schrödinger, LLC.

[42] B. R. Brooks, C. L. Brooks III, A. D. Mackerell Jr. L. Nilisson, R. J. Petrella, et al., *J. Comp. Chem.* **2009**, *30*, 1545-1614.

Entry for the Table of Contents

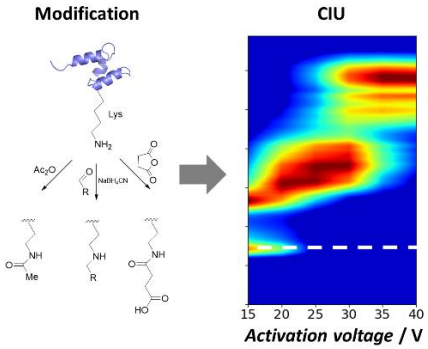

Native mass spectrometry is now widely used in protein structural studies. We present a methodology for probing the importance of specific residues in the stabilization of compact protein structure in the gas-phase using a combination of chemical modification and collision induced unfolding ion mobility-mass spectrometry.

Institute Twitter username: @NottsChemistry

WILEY-VCH